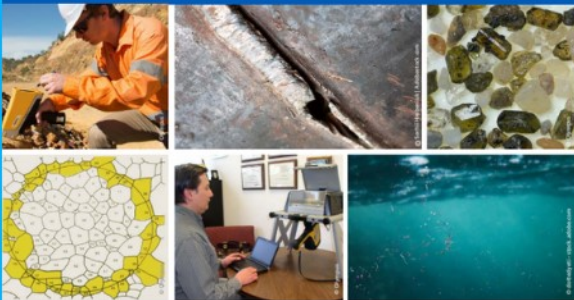




2nd Advanced Optical Metrology Compendium

Advanced Optical Metrology

Geoscience | Corrosion | Particles | Additive Manufacturing: Metallurgy, Cut Analysis & Porosity



EVIDENT
OLYMPUS

WILEY

The latest eBook from **Advanced Optical Metrology**.
Download for free.

This compendium includes a collection of optical metrology papers, a repository of teaching materials, and instructions on how to publish scientific achievements.

With the aim of improving communication between fundamental research and industrial applications in the field of optical metrology we have collected and organized existing information and made it more accessible and useful for researchers and practitioners.

EVIDENT
OLYMPUS

WILEY

Surface Modification of Fluorine-Doped Tin Oxide Thin Films Using Femtosecond Direct Laser Interference Patterning: A Study of the Optoelectronic Performance

Herman Heffner,* Marcos Soldera, Fabian Ränke, and Andrés Fabián Lasagni

Transparent conductive oxides (TCOs) are used in solar cells not only to extract photogenerated carriers but also to allow sunlight to reach the photoactive material. Therefore, controlling the electrical and optical properties of such oxides is crucial for the optimization of the efficiency of solar cells. Herein, direct laser interference patterning (DLIP) method is used to control the surface morphology, optical and electrical properties of fluorine-doped tin oxide (FTO) by applying femtosecond laser pulses. The topography characterization reveals periodic line-like microstructures with a period of 3.0 μm and average heights between 20 and 185 nm, depending on the applied laser fluence levels. Laser-induced periodic surface structures are observed on the valleys of the texture aligned perpendicularly to the laser radiation polarization. A relative increase in the average total and diffuse optical transmittance up to 5% and 500%, respectively, is obtained in the 400–800 nm spectral range as a consequence of the generated micro- and nanostructures. Calculations of two figures of merit suggest that the texturing of FTO might enhance the efficiency of solar cells, in particular dye-sensitized (DSSCs). The findings of this study confirm that DLIP is a convenient technique for structuring electrodes for highly efficient optoelectronic devices.


1. Introduction

The first transparent conductive oxide (TCO) was introduced by Karl Bädcker in 1907, more than 110 years ago.^[1] It was a

H. Heffner
Departamento de Química
Universidad Nacional del Sur, Instituto de Química del Sur (INQUISUR,
UNS-CONICET)
Av. Alem 1253, Bahía Blanca B800°CPB, Argentina
E-mail: herman.heffner@tu-dresden.de

H. Heffner, M. Soldera, F. Ränke, A. F. Lasagni
Institut für Fertigungstechnik
Technische Universität Dresden
George-Bähr-Str. 3c, 01069 Dresden, Germany

A. F. Lasagni
Fraunhofer-Institut für Werkstoff und Strahltechnik (IWS)
Winterbergstr 28, 01277 Dresden, Germany

 The ORCID identification number(s) for the author(s) of this article can be found under <https://doi.org/10.1002/adem.202201810>.

© 2023 The Authors. Advanced Engineering Materials published by Wiley-VCH GmbH. This is an open access article under the terms of the Creative Commons Attribution License, which permits use, distribution and reproduction in any medium, provided the original work is properly cited.

DOI: 10.1002/adem.202201810

thin film of cadmium oxide (CdO) prepared by oxidizing a vacuum-sputtered film of cadmium metal. By the same method, the first film of tin oxide (SnO_2) was obtained in 1937 by Gerhard Bauer.^[2] Currently, different TCOs are being employed in the optoelectronic industry such as aluminum-doped zinc oxide (AZO), indium-doped tin oxide (ITO), and fluorine-doped tin oxide (FTO). The latter has been extensively used as it possesses low fabrication costs compared to ITO because indium is a very scarce element on Earth,^[3] high thermal resistance, and good electronic compatibility with many semiconductors.^[4,5] To ensure the high performance of optoelectronic devices, two features are key for TCOs: high optical transmittance in the spectral range of interest and low electrical resistivity. Besides, a high level of diffuse spectral transmittance has been demonstrated to further enhance sunlight absorption in the photoactive material on many different solar cell

technologies.^[6–10] Particularly in FTO, numerous strategies were applied to achieve these goals, for instance, by changing the doping concentration of fluorine,^[11] by performing a surface chemical etching,^[12] by laser annealing,^[13] or by laser ablation.^[14,15] In the field of laser ablation, efforts have been carried out to develop different approaches to structure the surface without deteriorating the material's intrinsic properties, which could affect the optoelectronic performance of the device in which it will be employed. Saetang et al.^[16] structured FTO with an infrared (IR) ns-pulsed laser, generating line-like structures by means of a stream of water between the laser source and the conductive film. The results showed a reduction of the burr height index of 62.5% (relative) which is a critical parameter to reduce the intermittency between different thin layers in solar cells. Moreover, Kim et al.^[17] textured FTO for dye-sensitized solar cells (DSSCs) by using a continuous wave Nd:YAG infrared laser and obtained an 8.1% increase in the incident-photon-to-current efficiency (IPCE) compared to the solar cell based on unstructured FTO.

Regarding laser techniques, direct laser interference patterning (DLIP) has become an industrial-compatible technique able to produce large-area periodic surface micro- and nanostructures on a broad range of materials.^[18,19] Berger et al.^[20] used DLIP to structure ZnO:B thin films with an UV ns-laser and achieved a

3% (relative) increase in total transmittance (T_{tot}) and a 15% enhancement in diffuse transmittance (T_{diff}) for line-like structures with $1.5 \mu\text{m}$ of spatial period compared to the unstructured samples. This improvement was explained in terms of the triggering of diffraction modes caused by the produced surface pattern. Moreover, in recent previous studies, FTO thin films have been structured using DLIP, with infrared laser sources with 12^[14] and 0.9 ps pulses.^[15] In the case of the 12 ps pulses, an increase of up to 700% of the diffuse transmittance was obtained as a result of the periodic micro- and nanostructures, but the electrical resistance deteriorated due to the removal of conductive material as well. Thus, a tradeoff between optical and electrical properties was proposed. For the shorter pulse durations (0.9 ps), a similar increase in the diffuse transmittance was achieved; however, nonlinear optical effects generated a change in the electrode chemistry by aliovalent doping of Sn atoms that induced a transmittance loss in the blue spectral region. These effects are attempted to be solved in the present study using femtosecond pulses.

In this work, FTO thin films are patterned using direct laser interference patterning, applying a two-beam configuration and thus obtaining line-like periodic geometries using green laser wavelength and femtosecond pulses. The influence of the process parameters on the surface morphology, electrical and optical properties is studied and their potential impact on optoelectronic devices was addressed.

2. Experimental Section

2.1. DLIP of FTO Films

FTO thin films (550 nm thick) deposited on $25 \times 20 \times 3 \text{ mm}^3$ glass substrates (XOP Física, Spain) were used in this work. Prior to the laser treatment, each sample was cleaned with ethanol and dried with compressed air. A DLIP workstation (developed by TU Dresden and Fraunhofer IWS, Germany) equipped with a femtosecond solid-state laser (Carbide-40W-SH-TH, Light Conversion UAB, Lithuania) with a maximum pulse energy of $E_p = 400 \mu\text{J}$ was used to pattern the FTO substrates; the disposition along with the elliptical beam diameters ($2\omega_{0x}$ and $2\omega_{0y}$) can be seen in **Figure 1a**. The laser operated at a wavelength of $\lambda_L = 514 \pm 3 \text{ nm}$ with a pulse duration of $\tau_L = 280 \pm 2 \text{ fs}$ and a repetition rate of $f_L = 5 \text{ kHz}$. The DLIP optical module (x DLIP,

developed by TU Dresden and SurFunction GmbH, Germany) allows a single laser beam to be split, parallelized, and then focused on the sample (see **Figure 1b**) to perform the patterning experiments with an elliptical beam as a result.^[21] The DLIP optics provided two elongated laser beams with an intercepting angle θ of 9.85° , obtaining a spatial period Λ of $3.0 \mu\text{m}$.

The samples were translated in 2D directions (x and y) by a mechanical stage (Aerotech PRO155-05, USA). A pulse-to-pulse distance of $d_p = 500 \text{ nm}$ was used between the subsequent laser spots by controlling both the stage speed and repetition rate of the laser. The hatch distance h_d , which is the lateral distance between spots, was set to $153 \mu\text{m}$, while the fluence per pulse was varied from 780 to 900 mJ cm^{-2} .

2.2. Characterization Methods

In order to measure the surface topography of the structured FTO samples, a confocal microscope was used (CM, Sensofar S-Neox, Spain), using a $150\times$ magnification objective. The surface profiles and average height values of the topographies were obtained using SensoMAP Advanced Analysis Software (Sensofar, Spain). In addition, scanning electron microscopy (SEM) (Quattro ESEM, Thermo Fischer Scientific, Germany) analysis was performed at an acceleration voltage of 30 kV and the resulting images were analyzed with Gwyddion software.^[22]

Diffuse and total transmittances along with total reflectance were obtained using a UV-NIR spectrometer (HR 2000+, Ocean Optics, USA) with an integrating sphere (Thorlabs IS236A-4, Germany). Finally, electrical characterization of the structured samples was performed using the four-point probe method (gold coated tips, Coda Systems Ltd., UK), using an electrometer (SourceMeter 2450, Keithley, USA), and utilizing two different measurements modes, one perpendicular (transversal) to the direction of the pattern and the other one in the direction of the pattern (longitudinal). A total of five repetitions for each mode were done for statistical significance. By evaluating the ratio between the measured voltage V and the injected current I , a first approximation of the film resistance R was obtained. To calculate the effective sheet resistance (R_s), a correction factor of ≈ 0.90 was applied according to the National Bureau of Standards Technical Note 199 and contemplating the probe spacing ($\approx 1.8 \text{ mm}$) and the dimension of the sample ($\approx 5 \text{ cm}^2$).^[23]

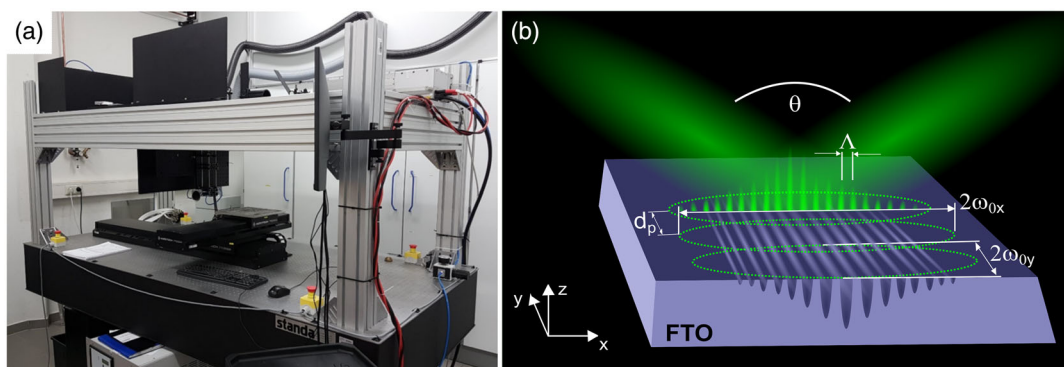


Figure 1. a) Laboratory workstation disposition and b) DLIP principle with an elliptical beam shape.

This adjustment is necessary because the proximity of boundaries might limit the current paths in the material. The values of R_S were then estimated using the expression $R_S = 4.5 \times 0.90 \times R$. Finally, it is worth mentioning that the determined R_S corresponds to an effective quantity that disregards the local variations of the film thickness produced after the DLIP process.

3. Results and Discussion

3.1. Topography Evolution upon Laser Structuring

In the first set of experiments, the pulse duration was varied between 280 fs and 1.0 ps in order to obtain the optimal pulse duration for which the FTO thin films can be patterned minimizing the amount of applied laser fluence. For these, the threshold fluence (F_{th}) was calculated by means of the D^2 method.^[24] This technique allows the indirect determination of the beam diameter and the material-dependent threshold fluence by measuring the diameter of the craters produced on the material by shooting laser pulses with different pulse energies.

The obtained results are presented in **Figure 2**, together with illustrative confocal microscopy images of the ablated areas for 280 fs and 1.0 ps at an approximate fluence level of $F = 3700 \text{ mJ cm}^{-2}$. As the pulse duration underwent from 280 fs to 1.0 ps, a linear increase in F_{th} was observed. This means that when using shorter pulse durations, lower fluence levels are required to ablate a given amount of material. As a consequence, the shorter used pulse duration permits to apply lower energy levels that allow a faster treatment (enhanced throughput) of the FTO film at a constant laser power level (average laser power). This finding is in accordance with previous research on diverse materials such as silicon, copper, gelatin, or borosilicate glass that had determined the linear relationship between the threshold fluence and the pulse duration.^[25,26] Thus, 280 fs laser pulses were chosen to carry out the experiments in this study.

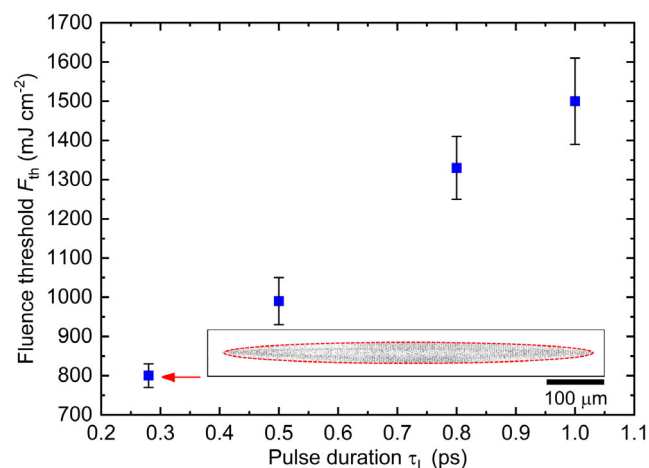


Figure 2. Ablation threshold fluence levels as a function of the pulse duration calculated by the D^2 method. The inset picture shows a confocal optical microscopy image of the elongated ablation spot ($690 \times 32 \mu\text{m}^2$) on the sample at a pulse duration of 280 fs.

In summary, the implementation of the D^2 method for a pulse duration of 280 fs yielded a fluence threshold of $F_{th} = 800 \pm 50 \text{ mJ cm}^{-2}$ and a beam radius along the long and short elliptical axes of $\omega_{0x} = 405 \pm 20 \mu\text{m}$ and $\omega_{0y} = 11.0 \pm 0.5 \mu\text{m}$, respectively.

For patterning the total area of the substrates, the fluence levels varied from 780 to 900 mJ cm^{-2} . In **Figure 3a–f**, topography images of DLIP-treated FTO thin films measured by confocal microscopy along with corresponding height profiles as a function of selected fluences (see caption) are shown. It is worth noting that for $F = 780 \text{ mJ cm}^{-2}$ no significant surface modifications were observed because the used fluences lay below the threshold value (see **Figure 2**), whereas for $F = 900 \text{ mJ cm}^{-2}$ severe deterioration of the texture quality was observed (not shown here) and thus these samples were disregarded. For the three highest fluence levels in **Figure 3a–c**, well-defined microchannels with a spatial period of $3.0 \mu\text{m}$ (which is in agreement with the period of the interference pattern provided by the x DLIP optical head) are observed with an average structure height between 75 and 185 nm. Surprisingly, the optimum fluence levels, i.e., approximately $840\text{--}860 \text{ mJ cm}^{-2}$, are slightly higher than the calculated threshold fluence of 800 mJ cm^{-2} . This can aim at multipulse ablation effects that might reduce the effective threshold fluence.^[27] More experiments should be done to demonstrate the validity of this statement.

The smoothness of the structure's sidewalls and the homogeneity of the textures can be qualitatively observed on each height profile. Additionally, to quantify the spikiness of the structures, kurtosis (Sku) was calculated. Higher values of Sku are related to a sharper distribution of the microstructures. Values between 3.0 and 4.6 (see labels in each subplot of **Figure 3**) were obtained for the three highest fluence levels. For lower values of laser fluence, not only smaller and less homogeneous microstructures were obtained (**Figure 3d–f**) but also higher values of Sku between 4.7 and 10.0 were estimated. This result points to the presence of sharper profiles with a relatively large number of high peaks and low valleys.^[28] Nonetheless, the line-like pattern could still be distinguished with average structure heights between 20 and 70 nm. No formation of laser-induced periodic surface structures (LIPSS) was observed in the confocal images because the lateral resolution provided by the used objective was 140 nm.

The measured average structure height as a function of the applied laser fluence is shown in **Figure 4**. In order to contrast the obtained threshold fluence value calculated previously by the D^2 method, a logarithmic fit using Equation (1) was performed using the measured average height of the microstructures (h) and the applied laser fluence (F), based on the model presented by Byskov–Nielsen et al.^[29] This relationship is indicated by Equation (1)

$$h = \frac{1}{\alpha} \ln \left(\frac{F}{F_{th}} \right) \quad (1)$$

This fitting, shown as a blue line in **Figure 4**, allows estimating the laser fluence threshold F_{th} of the FTO and the ratio $\frac{1}{\alpha}$, where α is the absorption coefficient at the laser wavelength. The logarithmic fitting curve yielded $F_{th} = 790 \pm 10 \text{ mJ cm}^{-2}$ and $\frac{1}{\alpha} = 1.93 \pm 0.10 \mu\text{m}$, the former being in close agreement with

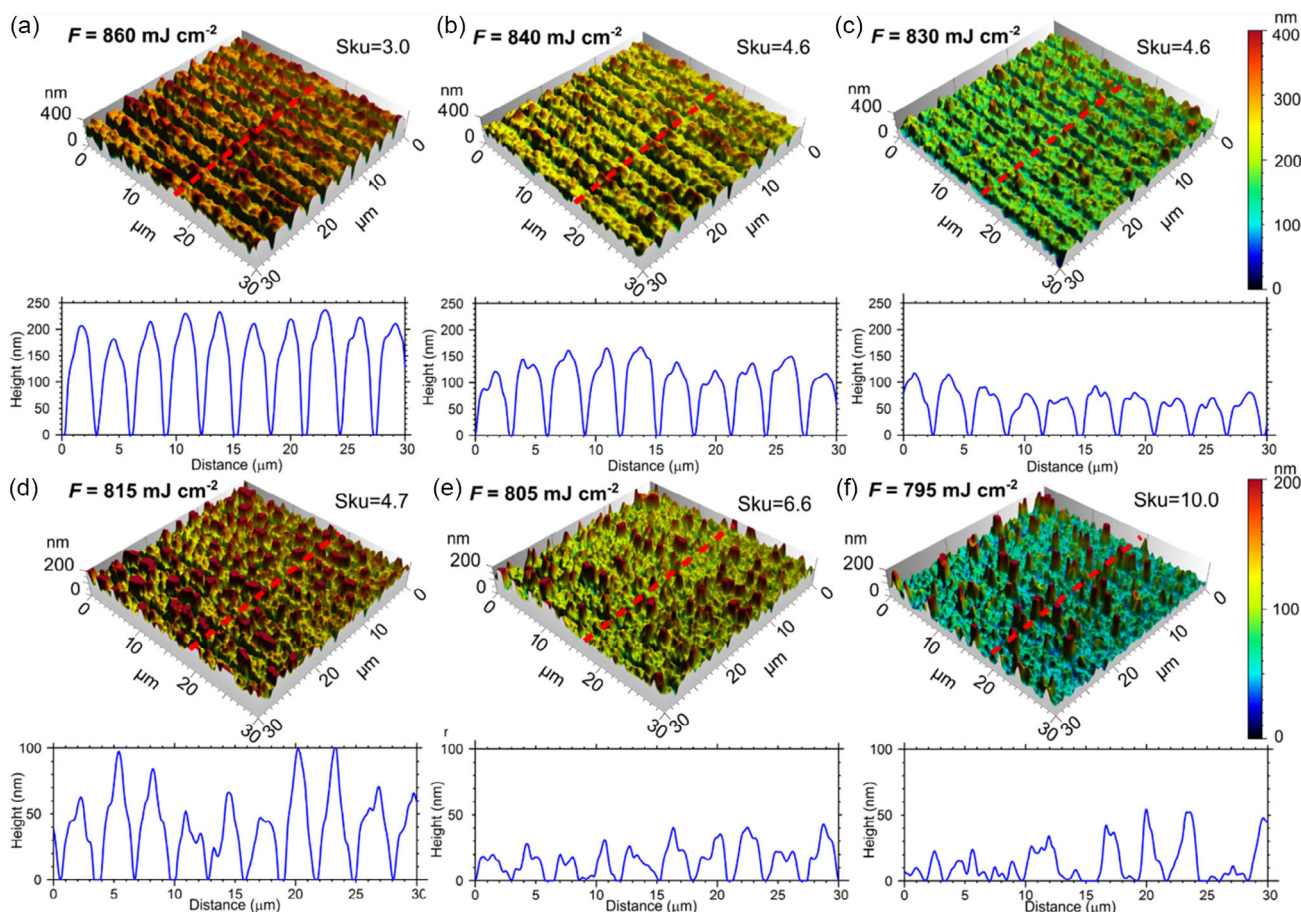


Figure 3. Confocal 3D views of structured FTO along with their average height profiles for fluence levels of a) 860 mJ cm^{-2} ; b) 840 mJ cm^{-2} ; c) 830 mJ cm^{-2} ; d) 815 mJ cm^{-2} ; e) 805 mJ cm^{-2} ; f) 795 mJ cm^{-2} . The red dashed lines mark where the profile was taken.

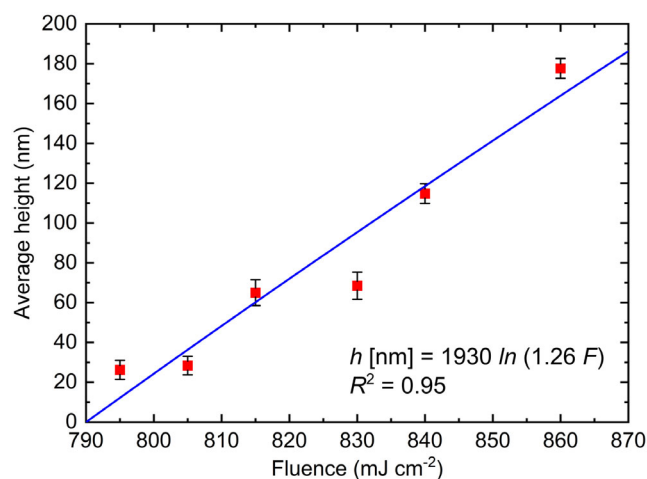


Figure 4. Measured average height of the microstructures as a function of the laser fluence, along with the logarithmic fit using Equation (1) (blue line).

the prior approximation of the value obtained by the D^2 method ($800 \pm 50 \text{ mJ cm}^{-2}$). In addition, the value found for $\frac{1}{\alpha}$ agrees

with prior investigations ($\frac{1}{\alpha}$ in the range of $1.3\text{--}2 \mu\text{m}$ at a wavelength of 514 nm).^[30,31]

In the interest of characterizing the surface features and evaluating the morphological changes that the surface treatment induced, an SEM analysis was performed. **Figure 5a** shows an SEM image of the untreated FTO surface, whereas **Figure 5b, c** displays SEM images of the DLIP-treated sample with $F = 860 \text{ mJ cm}^{-2}$. On the surface of the pristine FTO substrate (**Figure 5a**), randomly distributed nanocrystallites with a mean size of $370 \pm 86 \text{ nm}$ were observed. In the case of the microstructured surface, a line-like texture with a spatial period of $3.0 \mu\text{m}$ resulting from the DLIP treatment is visible. It can be observed that the nanocrystallites on the tops of the texture (corresponding to the intensity minima positions of the interference pattern) have the same morphology as in the untreated sample. Additionally, a mean crystallite size of $359 \pm 94 \text{ nm}$ was extracted, which is only 3% lower than in the reference sample. Thus, it can be considered that around the minima positions the fluence levels were low enough to prevent significant surface modifications. In turn, at the maxima positions not only ablation of the FTO material took place, but also the development of LIPSS was triggered. As a consequence, these positions match the valleys of the texture (**Figure 5b**). Furthermore, as the pulse

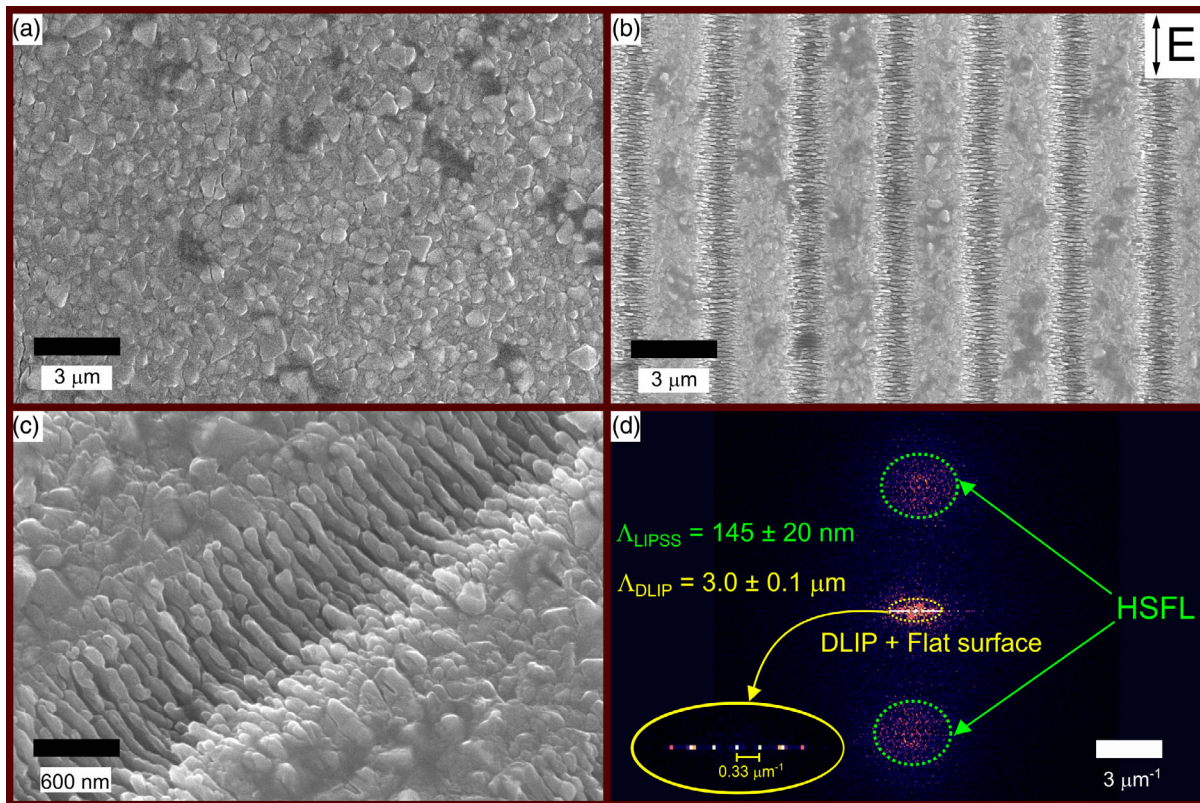


Figure 5. SEM images for a) untreated surface and b) patterned surface with a fluence level of $F = 860 \text{ mJ cm}^{-2}$ with the polarization direction of the electrical field; c) a tilted view of the ablated zone; d) the absolute value of 2D-FFT of Figure 5b with a zoomed view of the center frequencies. The double-lobes shapes corresponding to HSFL are denoted by green-dotted circles.

duration of the applied pulses was 280 fs, a thermal diffusion length of just 1 nm can be calculated in the FTO material considering a thermal diffusivity of $0.013 \text{ cm}^2 \text{ s}^{-1}$.^[32] This strongly suggests that cold ablation took place which is characterized by negligible heat-affected zones and therefore no noticeable metallurgical effects like recrystallization should have occurred at the maxima positions. The distribution of LIPSS perpendicular to the microchannels and polarization of the laser (indicated with the double arrow in Figure 5b) can be seen in more detail in the tilted view of Figure 5c. The absolute value of the 2D fast Fourier transform (2D-FFT) applied to Figure 5b is pictured in Figure 5d, showing the characteristic double-lobes shapes of LIPSS.^[33] A zoomed inset of the center of the spectrum shows the discrete spatial frequency peaks associated with the DLIP pattern. From the position of these features in the image, the spatial periods of the LIPSS and DLIP can be calculated, yielding $145 \pm 20 \text{ nm}$ and $3.0 \pm 0.1 \mu\text{m}$, respectively, for the sample structured with a fluence of $F = 860 \text{ mJ cm}^{-2}$.

The ratio between the measured spatial period corresponding to the LIPSS features and the laser wavelength is ≈ 0.3 which suggests that the LIPSS can be classified as high spatial frequency LIPSS (HSFL) because they are shorter than half of the used laser wavelength.^[34] This is in accordance with the study performed by Zhang et al., where femtosecond laser irradiation was applied in FTO thin films at different wavelengths. In that study, HSFL perpendicular to the polarization of the electrical

field and with a mean spatial period of 172 nm were obtained at a wavelength of 515 nm.^[35]

For a better understanding of the relationship between the laser fluence intensity and the period of the induced LIPSS, magnified SEM images of the generated HSFL for the highest four levels of applied laser fluence can be seen in Figure 6 (a: 860; b: 840; c: 830; and d: 815 mJ cm^{-2}). As the fluence decreases, the mean spatial period of the LIPSS also decreases. For example, at $F = 860 \text{ mJ cm}^{-2}$ and $F = 815 \text{ mJ cm}^{-2}$, the calculated spatial periods from the FFT analyses were 142 and 125 nm, respectively. This is in agreement with prior studies in which the same behavior has been observed for HSFL when the laser fluence (femtosecond pulses) was varied in very different material classes, such as glass, titanium, and carbon fibers.^[36–38]

3.2. Optical and Electrical Properties

To characterize the optical properties of structured FTO, total (T_{tot}) and diffuse (T_{diff}) transmittances along with total reflectance (R_{tot}) in the 400–800 nm spectral range were measured. Overall, the total transmittance for patterned FTO is lower than that of the flat reference in the 400–450 nm range as shown in Figure 7a. Remarkably, in the 450–800 nm range, all the patterned films show higher total transmittance compared to the untreated samples. In addition, as observed in Figure 7b, diffuse transmittance improves significantly after the DLIP

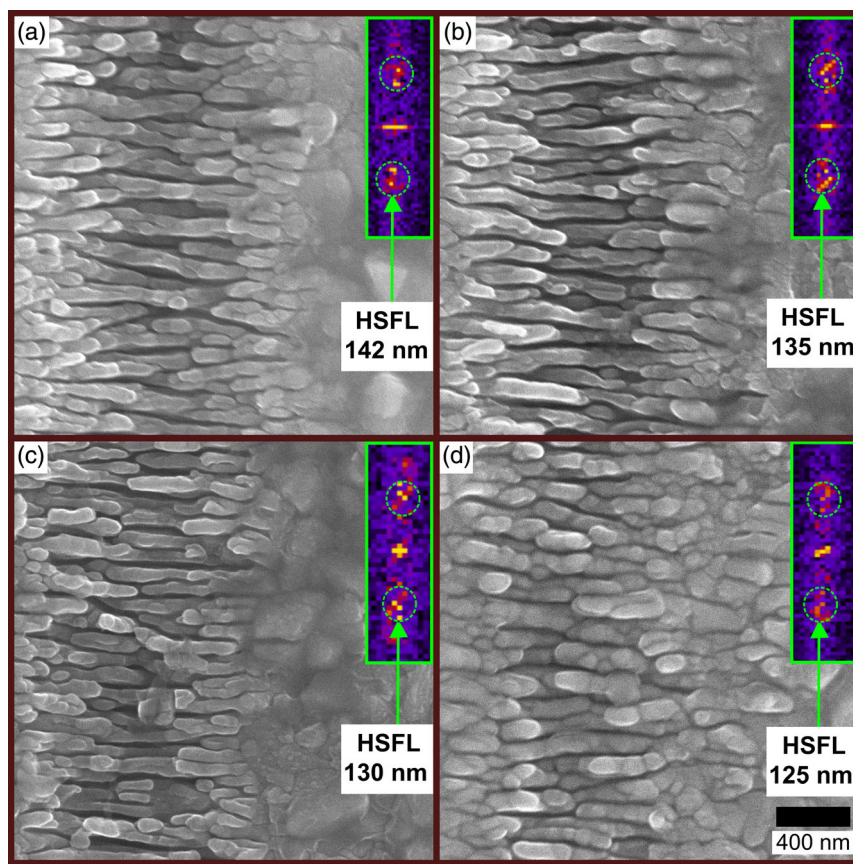


Figure 6. SEM images for treated surfaces at different fluence levels. The insets in each figure show the corresponding 2D-FFTs, for calculating the average spatial periods. Fluence levels: a) 860 mJ cm^{-2} ; b) 840 mJ cm^{-2} ; c) 830 mJ cm^{-2} ; and d) 815 mJ cm^{-2} .

treatment. Particularly, the film treated with a laser fluence of $F = 860 \text{ mJ cm}^{-2}$ exhibited the highest T_{diff} in the whole spectrum, exceeding 50% (absolute) in the 500–600 nm range.

Moreover, to quantify more precisely the obtained optical behavior of laser-treated surfaces, the average transmittances (total and diffuse), reflectance, and absorbance (A), defined as $A = 100\% - T_{\text{tot}} - R_{\text{tot}}$, obtained as a function of the fluence in the 400–800 nm spectral range are shown in **Table 1**. It is clear that the increase in the total transmittance is a result of a reduction of the average reflectance for all of the treated samples (up to 32.5% relative reduction for $F = 860 \text{ mJ cm}^{-2}$) and a decrease in the total absorbance (up to 15.5% relative reduction for $F = 840 \text{ mJ cm}^{-2}$). The reason behind these improvements might be related to two factors: 1) as FTO material was ablated without significantly inducing heat-affected zones around the ablated positions, there is a lower probability that light would be absorbed by the FTO because no degradation or recrystallization of the material is obtained; 2) HSFL with spatial periods shorter than the wavelength of visible light act as a material with a gradual effective refractive index, yielding a decrease in the total reflectance. The latter is in agreement with theoretical and experimental studies in which a significant reduction of the reflection was obtained with subwavelength structures on glass.^[39,40]

Furthermore, an increase (relative) in the average diffuse transmittance up to 500% was observed for the FTO film

structured at a fluence of $F = 860 \text{ mJ cm}^{-2}$ in comparison to the flat reference. In addition, comparable T_{tot} and T_{diff} behavior were obtained in our previous studies in which FTO thin films were structured by DLIP using infrared radiation with 12 and 0.9 ps pulses. In those studies, the total transmittance underwent a decrease in the 400–700 nm range and an increase in the 700–1000 nm range while diffuse transmittance reached an increment of up to 870% (relative) compared to unstructured FTO surface.^[14,15] However, in this work, a substantial increase in the average total transmittance was obtained for all the treated samples, reaching a 5.4% increase (relative) in T_{tot} for $F = 840 \text{ mJ cm}^{-2}$. This could enhance photon harvesting in optoelectronic devices in the vis–NIR spectrum or improve light out-coupling for light-emitting diodes.^[41]

In order to quantify the electrical effects that laser ablation induced on FTO thin films, the effective sheet resistance (R_s) as a function of the applied laser fluence is shown in **Figure 8a**. No significant differences between transversal and longitudinal modes were observed and thus the average values for both methods (transversal and longitudinal) are presented. A linear increase in R_s was observed as the laser fluence increased. This was the result of the removal of conductive material at the interference maxima positions which induced an increase in the film resistance. For the lowest fluence value of 795 mJ cm^{-2} , a sheet resistance $R_s = 7.8 \Omega \text{ sq}^{-1}$ was achieved

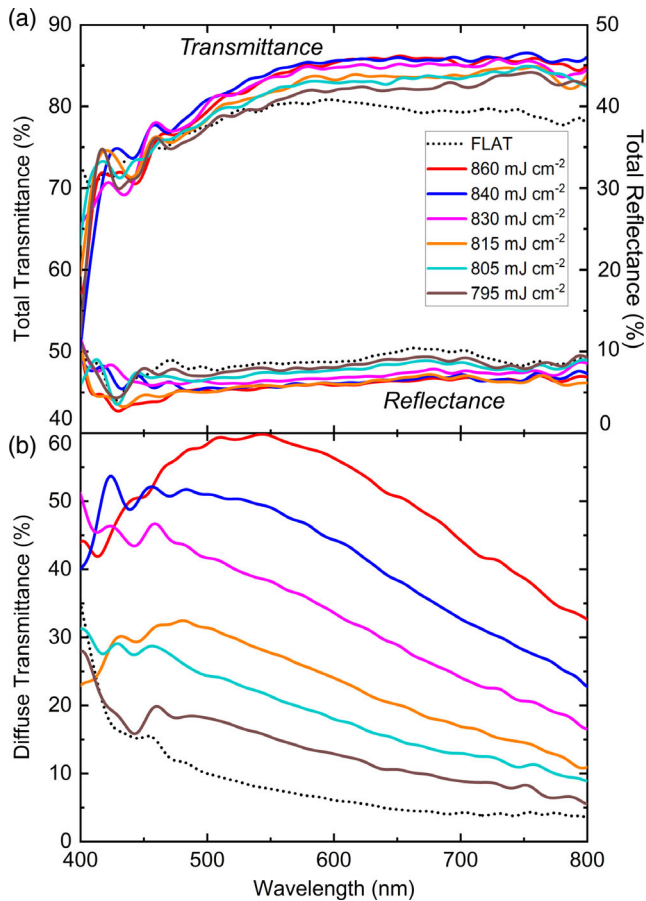


Figure 7. a) Total transmittance, reflectance, and b) diffuse transmittance for selected fluence levels. The dotted lines indicate the values for untreated FTO.

Table 1. Calculated average total transmittance, reflectance, diffuse transmittance, and absorbance in the 400–800 nm spectral range for each fluence level. Values in brackets indicate the relative deviation in percentage with reference to the untreated FTO film.

F [mJ cm ⁻²]	\bar{T}_{tot} [%]	\bar{R}_{tot} [%]	\bar{T}_{diff} [%]	\bar{A} [%]
Ref.	78.2	8.6	8.2	13.2
795	79.7 (+1.9)	8.0 (-7.0)	13.2 (+60)	12.3 (-6.8)
805	80.8 (+3.3)	7.6 (-11.6)	18.7 (+130)	11.6 (-12.1)
815	80.9 (+3.4)	5.9 (-31.4)	22.8 (+180)	13.2 (+0)
830	81.7 (+4.5)	7.0 (-18.6)	32.9 (+300)	11.3 (-14.4)
840	82.4 (+5.4)	6.4 (-25.6)	41.1 (+400)	11.2 (-15.5)
860	81.9 (+4.7)	5.8 (-32.5)	49.5 (+500)	12.3 (-6.8)

which represents an increase of 10% (relative) compared to the untreated surface. On the other hand, for the highest fluence of 860 mJ cm⁻² a sheet resistance $R_s = 11.3 \Omega \text{ sq}^{-1}$ was measured corresponding to a 50% (relative) increase. In this regard, a former study conducted by Wang et al.^[42] suggest that the surface texturing of FTO thin films induces an increment up to 16% (relative) of the efficiency in DSSCs as long as the sheet

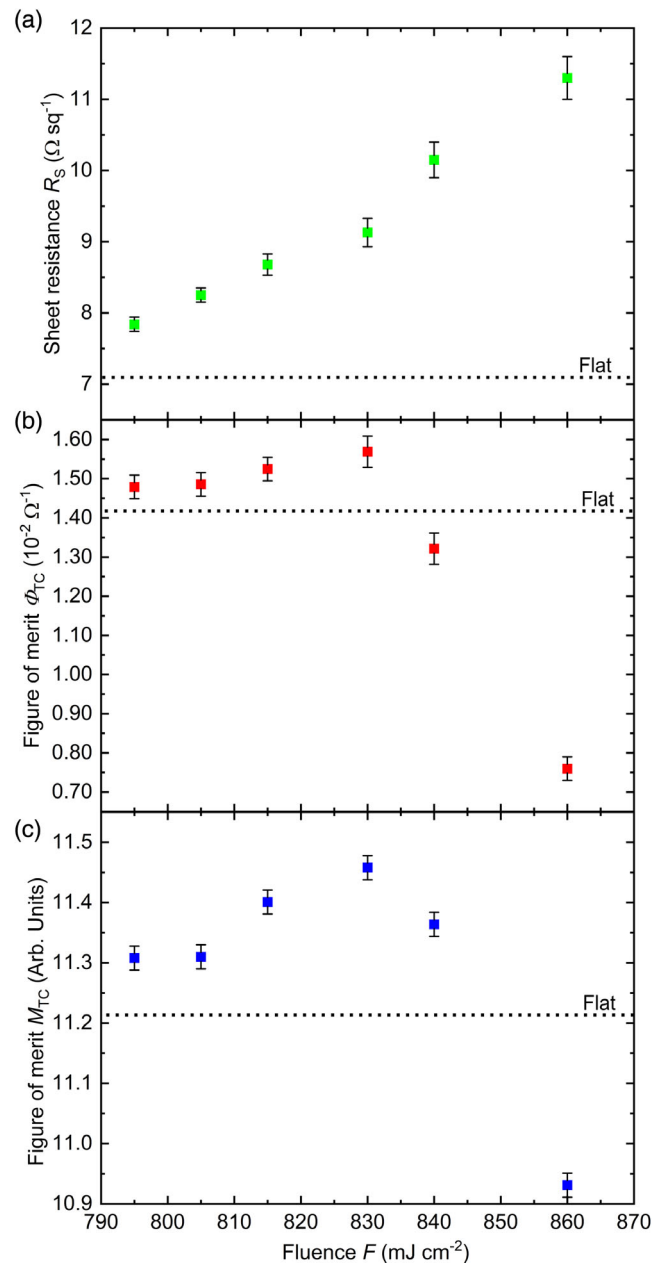


Figure 8. a) Effective sheet resistance and figures of merit b) Φ_{TC} and c) M_{TC} as a function of the applied laser fluence. The dotted lines indicate the values for untreated FTO.

resistance remains below $27 \Omega \text{ sq}^{-1}$. This means that all patterned FTO thin films in this study could be suitable for DSSCs.

To analyze the overall performance of transparent conductors (TC) in solar cells, Haacke et al.^[43] introduced a figure of merit (Φ_{TC}) defined by Equation (2)

$$\Phi_{TC} = \frac{\hat{T}_{\text{tot}}^{10}}{R_s} \quad (2)$$

where R_s is the average effective sheet resistance, which in our case was measured with the four-point probe method

(see Experimental Section for details) and \hat{T}_{tot} is the average total transmittance in the 400–800 nm range weighted by the solar standard spectral irradiance AM1.5G using Equation (3)

$$\hat{T}_{\text{tot}} = \frac{\int_{400 \text{ nm}}^{800 \text{ nm}} I(\lambda)_{\text{AM1.5G}} \times T_{\text{tot}}(\lambda) d\lambda}{\int_{400 \text{ nm}}^{800 \text{ nm}} I(\lambda)_{\text{AM1.5G}} d\lambda} \quad (3)$$

Here, the lower limit of 400 nm was selected due to the limitation imposed by our spectrometer setup, whereas the highest limit of 800 nm coincides with the absorption onset of many thin film absorbers such as polymeric small molecular weight and perovskite semiconductors.^[44,45] Originally, Equation (2) was designed to employ only the total transmittance value at 550 nm because it is the wavelength that corresponds to the maximum of the solar spectral irradiance. However, to obtain a more realistic figure of merit, the average weighted transmittance in the mentioned spectral range was used.^[46]

The results are shown in Figure 8b, in which the figure of merit Φ_{TC} is illustrated as a function of the applied laser fluence. The figure of merit for the flat surface is $\Phi_{\text{TC}} \approx 1.43 \times 10^{-2}$ which is comparable with the value of $\Phi_{\text{TC}} \approx 1.11 \times 10^{-2}$ obtained by Purwanto et al.^[47] on FTO with a film thickness of ≈ 260 nm. For fluence levels between 795 and 830 mJ cm^{-2} , the figure of merit is above the level of unstructured FTO, meaning a possible improvement in the overall performance of the solar cell when it is treated with the DLIP method. For higher fluence levels, the performance decays most likely because the higher sheet resistance values are dominant compared to the improvements in the optical properties.

Particularly for dye-sensitized solar cells, Huang et al.^[48] defined also a figure of merit by adjusting experimental data of ruthenium-based DSSCs according to

$$M_{\text{TC}}(R_S, \hat{T}_{\text{tot}}) = (0.769 - 0.0868 \times \hat{T}_{\text{tot}} - 0.000287 \times R_S - 0.00207 \times \hat{T}_{\text{tot}} \times R_S) \times (1.23 + 18.99 \times \hat{T}_{\text{tot}}) \quad (4)$$

This expression is linearly related to the efficiency of DSSCs, thus a higher figure of merit M_{TC} could imply a higher performance of the device. In Figure 8c, the calculated M_{TC} values are presented as a function of the applied laser fluence. The highest value of $M_{\text{TC}} = 11.46$ was obtained for an applied laser fluence of $F = 830 \text{ mJ cm}^{-2}$ and is also comparable with the value that Mrabet et al.^[49] obtained for lanthanum-doped tin oxide. This represents an increment (relative) of 2.2% compared to the unstructured FTO which could also imply a similar rise in the efficiency for ruthenium-based DSSCs.

In consequence, both figures of merit present an improvement in textured FTO thin films at moderate laser fluence levels, even though the removal of conductive material induced an increment of the effective sheet resistance values. Moreover, considering the effects of the increase of the effective surface area of FTO along with the scattering of incident light induced by the periodic microstructures, further efficiency improvement can be expected. For instance, Li et al.^[50] developed textured FTO electrodes for perovskite solar cells using laser etching. Even

though a sheet resistance of $R_S = 22.0 \text{ sq}^{-1}$ was obtained, an increase of efficiency of up to 13% (relative) compared to the device based on untreated FTO was achieved. This was the result of not only the enhancement produced by better light trapping capabilities but also due to a decrease in the recombination resistance in the FTO/TiO₂/CH₃NH₃PbI₃ interfaces resulting from the increase in the effective surface area. In addition, Kong et al.^[51] indicated that using textured FTO promotes a higher contact area between the front FTO electrode and the electron transport layer (TiO₂) in DSSCs, which enhances the charge transfer and ultimately the efficiency.

4. Conclusions

In this work, the morphological, optical, and electrical modifications induced by DLIP based on a green femtosecond-pulsed source on FTO thin films were studied. As the laser fluence increased from 795 to 860 mJ cm^{-2} , the FTO film progressed from a marginal surface modification to the formation of well-defined microchannels decorated with high spatial frequency LIPSS with spatial periods between 125 and 165 nm. As expected from previous studies on other materials, a linear trend was found between the pulse duration and the ablation fluence threshold in the studied range of pulse durations (280 fs to 1.0 ps). The total and diffuse transmittances were enhanced by a relative 5% and 500%, respectively, as a result of the diffraction of incident light induced by the periodic texture combined with the presence of the nanoscaled LIPSS. Additionally, empirical figures of merit Φ_{TC} and M_{TC} suggest that the optoelectronic performance of DSSCs might be enhanced if FTO is structured with an applied laser fluence near the threshold level. Moreover, it is expected further improvements in the efficiency of such devices due to the increase of the effective surface area of the electrode could be advantageous for a more effective charge transfer between the electrode and TiO₂ and an increased light harvesting in the red and near-infrared spectra.

Acknowledgements

H.H. acknowledges the Argentinian Ministry of Education as well as the German Academic Exchange Service (DAAD) for supporting this work. The authors would like to thank TOPAG GmbH for providing a state-of-the-art laser system to TU Dresden for conducting the microtexturing experiments.

Open Access funding enabled and organized by Projekt DEAL.

Conflict of Interest

The authors declare no conflict of interest.

Author Contributions

H.H.: Conceptualization, investigation, formal analysis, data curation, visualization, methodology (samples structuring; topography, optical and electrical characterization), writing—original draft; M.S.: methodology (SEM imaging), validation, supervision, writing—review and editing; F.R.: methodology (design and implementation of DLIP setup and elongated beam calibration); A.F.L.: conceptualization, methodology, resources, supervision, Writing—review and editing, funding acquisition.

Data Availability Statement

The data that support the findings of this study are available from the corresponding author upon reasonable request.

Keywords

direct laser interference patterning, femtosecond laser, fluorine-doped tin oxide, solar cells, surface texturing

Received: December 14, 2022

Revised: January 28, 2023

Published online:

- [1] K. Bädeker, *Ann. Phys.* **1907**, 327, 749.
- [2] G. Bauer, *Ann. Phys.* **1937**, 422, 433.
- [3] M. Lokanc, R. Eggert, M. Redlinger, *The Availability of Indium: The Present, Medium Term, and Long Term*, National Renewable Energy Lab. (NREL), Golden, CO **2015**.
- [4] S. Sheehan, P. K. Surolia, O. Byrne, S. Garner, P. Cimo, X. Li, D. P. Dowling, K. R. Thampi, *Sol. Energy Mater. Sol. Cells* **2015**, *132*, 237.
- [5] D.-J. Kwak, B.-H. Moon, D.-K. Lee, C.-S. Park, Y.-M. Sung, *J. Electr. Eng. Technol.* **2011**, *6*, 684.
- [6] L. Forbes, *Sol. Energy* **2012**, *86*, 319.
- [7] M. Soldera, K. Taretto, J. Berger, A. F. Lasagni, *Adv. Eng. Mater.* **2016**, *18*, 1674.
- [8] Q. Rong, J. Zhao, H. Yu, N. Li, Q. Zhang, D. Yuan, W. Liu, D. Zheng, X. Gao, L. Shui, G. Zhou, L. Nian, *J. Mater. Chem. C* **2019**, *7*, 8515.
- [9] J. Wu, X. Che, H.-C. Hu, H. Xu, B. Li, Y. Liu, J. Li, Y. Ni, X. Zhang, X. Ouyang, *J. Mater. Chem. A* **2020**, *8*, 5442.
- [10] Y. Lei, Y. Li, Z. Jin, *Energy Rev.* **2022**, *1*, 100003.
- [11] C.-C. Lin, M.-C. Chiang, Y.-W. Chen, *Thin Solid Films* **2009**, *518*, 1241.
- [12] J.-W. Bae, B.-R. Koo, H.-R. An, H.-J. Ahn, *Ceram. Int.* **2015**, *41*, 14668.
- [13] B. Li, G. Yang, L. Huang, W. Zu, H. Li, Y. Wang, S. Li, N. Ren, *Mater. Res. Bull.* **2018**, *108*, 151.
- [14] H. Heffner, M. Soldera, A. F. Lasagni, *Adv. Eng. Mater.* **2022**, *24*, 2200266.
- [15] H. Heffner, M. Soldera, F. Schell, M. Deconinck, Y. Vaynzof, L. E. Mulko, A. Lasagni, *J. Mater. Chem. C* **2022**, *10*, 17954.
- [16] V. Saetang, H. Qi, T. Smerchit, N. Rujisamphan, *Opt. Laser Technol.* **2022**, *153*, 108280.
- [17] H.-J. Kim, M.-S. Lee, D.-G. Lee, M.-K. Son, K.-J. Lee, *Opt. Lasers Eng.* **2009**, *47*, 558.
- [18] L. Mulko, M. Soldera, A. F. Lasagni, *Nanophotonics* **2021**, *11*, 203.
- [19] D. W. Müller, S. Lößlein, C. Pauly, M. Briesenick, G. KICKelbick, F. Mücklich, *Appl. Surf. Sci.* **2022**, *611*, 155538.
- [20] J. Berger, T. Roch, S. Correia, J. Eberhardt, A. F. Lasagni, *Thin Solid Films* **2016**, *612*, 342.
- [21] A. F. Lasagni, B. Voisiat, Arrangement of Optical Elements for the Formation of Large-Area Structures with Linear Structural Elements, *DE102020204656A1* 14 October **2021**.
- [22] D. Nečas, P. Klapetek, *Open Phys.* **2012**, *10*, 181.
- [23] L. J. Swartzendruber, U. S. N. B. of Standards, *Correction Factor Tables for Four-Point Probe Resistivity Measurements on Thin, Circular Semiconductor Samples*, U.S. Department of Commerce, National Bureau of Standards, Washington, D.C. **1964**.
- [24] Y. C. Kiang, R. W. Lang, *Appl. Opt.* **1983**, *22*, 1296.
- [25] C. S. R. Nathala, A. Ajami, W. Husinsky, B. Farooq, S. I. Kudryashov, A. Daskalova, I. Bliznakova, A. Assion, *Appl. Phys. A* **2016**, *122*, 107.
- [26] W. Kautek, J. Krüger, M. Lenzner, S. Sartania, C. Spielmann, F. Krausz, *Appl. Phys. Lett.* **1996**, *69*, 3146.
- [27] R. D. Palo, A. Volpe, C. Gaudiuso, P. Patimisco, V. Spagnolo, A. Ancona, *Opt. Express* **2022**, *30*, 44908.
- [28] E. S. Gadelmawla, M. M. Koura, T. M. A. Maksoud, I. M. Elewa, H. H. Soliman, *J. Mater. Process. Technol.* **2002**, *123*, 133.
- [29] J. Byskov-Nielsen, J.-M. Savolainen, M. S. Christensen, P. Balling, *Appl. Phys. A* **2010**, *101*, 97.
- [30] N. A. Bakr, S. A. Salman, M. N. Ali, *Adv. Mater.* **2016**, *5*, 23.
- [31] S. B. Ameer, A. Barhoumi, H. Bel hadjtaief, R. Mimouni, B. Duponchel, G. Leroy, M. Amlouk, H. Guermazi, *Mater. Sci. Semicond. Process.* **2017**, *61*, 17.
- [32] S.-F. Tseng, W.-T. Hsiao, D. Chiang, C.-K. Chung, J.-L. Andrew Yeh, *Opt. Laser Technol.* **2014**, *52*, 212.
- [33] S. Rung, S. Schwarz, B. Götzendorfer, C. Esen, R. Hellmann, *Appl. Sci.* **2018**, *8*, 700.
- [34] J. Bonse, S. Höhm, S. V. Kirner, A. Rosenfeld, J. Krüger, *IEEE J. Sel. Top. Quantum Electron.* **2017**, *23*, 9000615.
- [35] F. Zhang, L. Chen, Y. Zhang, Q. Jiang, D. Feng, S. Zhang, T. Jia, Z. Sun, H. Xu, *Front. Phys.* **2022**, *10*, 208.
- [36] S. Höhm, A. Rosenfeld, J. Krüger, J. Bonse, *J. Appl. Phys.* **2012**, *112*, 014901.
- [37] C. S. R. Nathala, A. Ajami, A. A. Ionin, S. I. Kudryashov, S. V. Makarov, T. Ganz, A. Assion, W. Husinsky, *Opt. Express* **2015**, *23*, 5915.
- [38] C. Kunz, T. N. Büttner, B. Naumann, A. V. Boehm, E. Gnecco, J. Bonse, C. Neumann, A. Turchanin, F. A. Müller, S. Gräf, *Carbon* **2018**, *133*, 176.
- [39] C. L. Pinto, I. Cornago, A. Buceta, E. Zugasti, J. Bengoechea, *Sol. Energy Mater. Sol. Cells* **2022**, *236*, 111506.
- [40] C. L. Pinto, I. Cornago, A. Buceta, E. Zugasti, J. Bengoechea, *Sol. Energy Mater. Sol. Cells* **2022**, *246*, 111935.
- [41] W. Wang, L. Qi, *Adv. Funct. Mater.* **2019**, *29*, 1807275.
- [42] F. Wang, N. K. Subbaiyan, Q. Wang, C. Rochford, G. Xu, R. Lu, A. Elliot, F. D'Souza, R. Hui, J. Wu, *ACS Appl. Mater. Interfaces* **2012**, *4*, 1565.
- [43] G. Haacke, *J. Appl. Phys.* **1976**, *47*, 4086.
- [44] J. Du, K. Hu, J. Zhang, L. Meng, J. Yue, I. Angunawela, H. Yan, S. Qin, X. Kong, Z. Zhang, B. Guan, H. Ade, Y. Li, *Nat. Commun.* **2021**, *12*, 5264.
- [45] M. Albaladejo-Siguan, D. Becker-Koch, A. D. Taylor, Q. Sun, V. Lami, P. G. Oppenheimer, F. Paulus, Y. Vaynzof, *ACS Nano* **2020**, *14*, 384.
- [46] T. M. Barnes, M. O. Reese, J. D. Bergeson, B. A. Larsen, J. L. Blackburn, M. C. Beard, J. Bult, J. van de Lagemaat, *Adv. Energy Mater.* **2012**, *2*, 353.
- [47] A. Purwanto, H. Widiyandari, A. Jumari, *Thin Solid Films* **2012**, *520*, 2092.
- [48] X. Huang, Y. Zhang, H. Sun, D. Li, Y. Luo, Q. Meng, *J. Renewable Sustainable Energy* **2009**, *1*, 063107.
- [49] C. Mrabet, A. Boukhachem, M. Amlouk, T. Manoubi, *J. Alloys Compd.* **2016**, *666*, 392.
- [50] J. F. Li, H. Y. Hao, J. B. Hao, L. Shi, J. J. Dong, H. Liu, J. Xing, *IOP Conf. Ser.: Mater. Sci. Eng.* **2019**, *479*, 012046.
- [51] S. M. Kong, Y. Xiao, K. H. Kim, W. In Lee, C. W. Chung, *Thin Solid Films* **2011**, *519*, 3173.